ACS APPLIED MATERIALS & INTERFACES

Research Article

www.acsami.org

Comparative Degradation and Regeneration of Polymer Solar Cells with Different Cathodes

Pankaj Kumar,*[,†,‡] Chhinder Bilen,[‡] Krishna Feron,[‡,§] Nicolas C. Nicolaidis,[‡,§] Bill B. Gong,[∥] Xiaojing Zhou,[‡] Warwick J. Belcher,[‡] and Paul C. Dastoor*[,‡]

[†]CSIR-National Physical Laboratory, Dr. K. S. Krishnan Marg, New Delhi 110012, India

[‡]Centre for Organic Electronics, University of Newcastle, Callaghan, NSW 2308, Australia

[§]CSIRO Energy Technology, P.O. Box 330, Newcastle, NSW 2300, Australia

[∥]Mark Wainwright Analytical Centre, University of New South Wales, Sydney, NSW 2052, Australia

ABSTRACT: A comparative degradation study of solar cells based on a bulk-heterojunction (BHJ) blend of poly(3-hexylethiophene) (P3HT) and phenyl [6,6] C_{61} butyric acid methyl ester (PCBM) with two different cathodes is reported. Poly(ethylene-dioxythiphene):poly(styrene sulfonate) (PEDOT:PSS) coated ITO electrodes were used as the anode, whereas Ca/Al and Ca/Ag electrodes were used as cathodes. Fully degraded devices were subjected to thermal annealing under inert atmosphere. The performance of degraded solar cells with a Ca/Al cathode exhibited no improvement after treatment. However the solar cells with a Ca/Ag cathode exhibited a considerable recovery in their performance following annealing under a nitrogen atmosphere. Indeed, these solar cells could be subjected to many degradation and regeneration cycles. Current density−voltage (*J-V*) characteristics and X-ray photoelectron spectroscopy (XPS) studies show that this behavior arises from the complex chemical thermodynamics of the reactions that can occur at the cathode/active layer interface. In particular, the recovery of device performance for solar cells with a Ca/Ag cathode is due to the reversible oxidation of Ag upon thermal annealing.

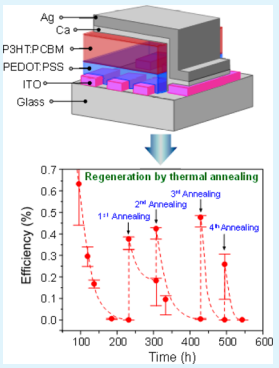

KEYWORDS: *polymer solar cells, regeneration, thermal annealing, P3HT, PCBM*

1. INTRODUCTION

Polymer solar cells (PSCs) possess many advantageous properties such as their thin, lightweight, transparent nature and their cost-effective manufacturing via high-throughput roll to roll production.[1] Over the past two decades PSCs have experienced a rapid growth in performance, with the donor−acceptor bulk-heterojunction (BHJ) architecture proving to be the most successful design.[2−5] Through sophisticated modification of energy band-gaps, energy levels, morphology, and interfaces of the active materials, PSCs have demonstrated power conversion efficiencies (PCEs) exceeding 10%.[2−7] Module cost calculations show that PSCs with lifetimes of 5−10 years and efficiencies 8−10% are predicted to produce electricity at ∼10 Eurocents/kWh.[8,9] Although considerable progress has been made toward the required PCE target, the poor stability of PSCs is now a major concern, and, in order to realize the full potential of this technology, the long-term stability of these devices must be improved further. As such, degradation in PSCs has now become an important area of research for both the academia and industry. A number of reports have demonstrated that diffusion of O_2 and H_2O molecules into PSCs has the most detrimental effect on device operation.[10−14] These molecules react with almost every component of a PSC resulting in electrode oxidation, interface degradation, morphological changes and electrophotochemical reactions, which degrade their optical and electronic properties.[15−19] Although O_2 and H_2O molecules can migrate through the edges and top surface of the devices, macroscopic pin holes in the top electrodes are thought to provide the main diffusion pathway.[20,21]

Here we report degradation studies of P3HT:PCBM solar cells with two different cathodes (Ca/Al and Ca/Ag). The initial goal of this study was to probe the effect of oxidation processes upon these two device cathode structures. However, the results of this study revealed that the oxidation processes in PSC devices are much more complex than previously thought. In particular, device characterization and XPS depth profiling show that cathode degradation consists of a series of both irreversible and *reversible* processes. Furthermore, by manipulating these processes we are able to recover the performance of degraded devices. The manuscript is organized as follows. First, we discuss the chemical thermodynamics of cathode degradation in relation to Ca/Al and Ca/Ag cathodes. Consequently, we predict that it should be possible to reverse certain degradation (oxidation) processes for Ca/Ag cathodes under the typical experimental conditions used in device processing. Finally, we present experimental evidence showing that partial recovery of PSC performance does indeed occur where these reversible oxidation processes are accessible.

Received: January 28, 2014
Accepted: March 13, 2014
Published: March 13, 2014

   dx.doi.org/10.1021/am500637n | *ACS Appl. Mater. Interfaces* 2014, 6, 5281−5289

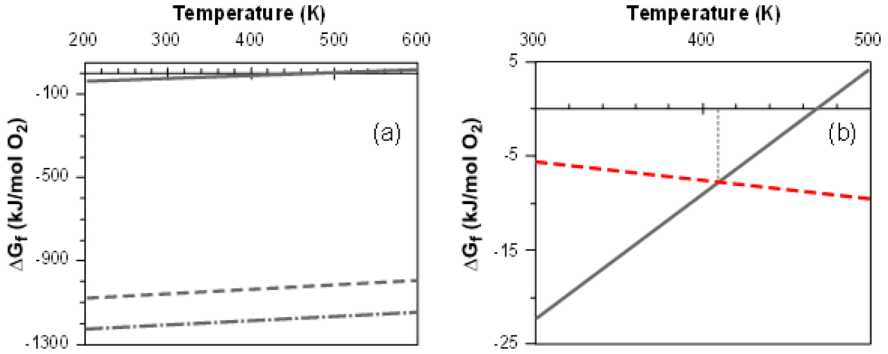

Figure 1. (a) Ellingham diagram for oxidation of Ca (dash-dotted line), Al (dashed line), and Ag (solid line). (b) Ellingham diagram for the oxidation of Ag (solid line) together with the free energy line for a partial pressure of O_2 of 10^{-4} kPa (dashed line). The intercept of the two lines indicates the equilibrium oxidation temperature for the formation of Ag_2O (dotted line).

2. CHEMICAL THERMODYNAMICS OF CATHODE DEGRADATION

It is widely accepted that the oxidation of the cathode electrode plays a key role in the degradation of PSCs, with typical cathode electrodes comprising metals such as Al or Ag with Ca as an interfacial layer.[22,23]

The most relevant atmospheric oxidation reactions for these materials can be given by the following equations:

$$2Ca + O_2 \rightarrow 2CaO \quad (1)$$

$$Ca + H_2O \rightarrow CaO + H_2 \quad (2)$$

$$CaO + H_2O \leftrightarrow Ca(OH)_2 \quad (3)$$

$$4Ag + O_2 \leftrightarrow 2Ag_2O \quad (4)$$

$$2Ag + H_2O \rightarrow Ag_2O + H_2 \quad (5)$$

$$4Al + 3O_2 \rightarrow 2Al_2O_3 \quad (6)$$

$$2Al + 3H_2O \rightarrow Al_2O_3 + 3H_2 \quad (7)$$

The chemical thermodynamics of an oxidation reaction determines the relative ease of that oxidation pathway for a given metal and is commonly presented in the form of an Ellingham diagram.[24] These diagrams plot the Gibbs free energy of formation per mole of oxygen consumption (ΔG_f) as a function of temperature and are typically used in metallurgy to determine preferential oxidation in mixed metal systems (such as alloys).[25] The Ellingham diagrams for the reaction of the three metal electrode materials with oxygen in the solid state (Figure 1 (a)) show that the order of oxidation preference at all temperatures is Ca, Al, and Ag. Moreover, from Figure 1(b) we see that at a partial pressure of O_2 of 10^{-4} kPa (~1 ppm) the equilibrium oxidation temperature for Ag_2O is lowered from its value of 462 K (189 °C) under ambient conditions to 409 K (136 °C). The oxidation of these metal electrodes can also occur through interaction with water.[22] In the case of Ca, this reaction is much more facile than the oxygen reaction and dominates the oxidation process under typical atmospheric conditions.[26]

In addition, CaO readily undergoes a further hydrolysis reaction in the presence of water to produce $Ca(OH)_2$ (eq 3), whereas Ag_2O and Al_2O_3 are generally chemically inert to hydrolysis under ambient conditions. Work by Schaube et al. has shown that the equilibrium temperature for eq 3 can be written as[27]

$$\ln\left(\frac{P_{eq}}{10^5}\right) = \frac{-12845}{T_{eq}} + 16.508 \quad (8)$$

where P_{eq} is the equilibrium partial pressure of H_2O in Pa, and T_{eq} is the equilibrium temperature in K.

Figure 2 shows that as the partial pressure of water drops so the equilibrium temperature of the CaO hydrolysis reaction

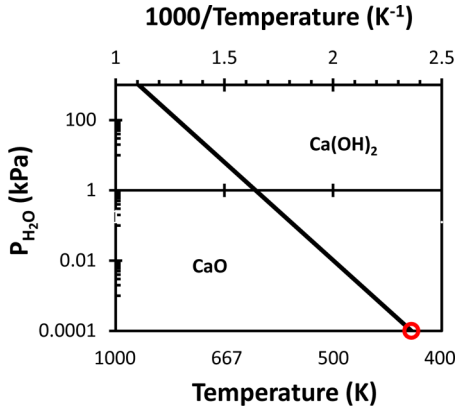

Figure 2. Variation in the equilibrium temperature of CaO hydrolysis reaction as a function of partial pressure of water. The open red circle indicates the equilibrium temperature (424 K) at a partial pressure of H_2O of 10^{-4} kPa.

also decreases. Moreover, at a partial pressure of H_2O of 10^{-4} kPa (~1 ppm) the equilibrium temperature for CaO hydrolysis is lowered to a value of 424 K (151 °C). This analysis reveals that not all of the oxidative processes that occur during degradation of the PSC cathodes are irreversible. Thus, while Al_2O_3 and CaO readily form at all temperatures, Ag_2O will convert back to Ag at ~140−150 °C under conditions of low relative O_2 concentration. Likewise, under dry conditions the hydrolysis of $Ca(OH)_2$ is reversed at similar temperatures. PSC fabrication is typically conducted under an inert atmosphere (with O_2 and H_2O concentrations kept below 1 ppm) with processing conditions (such as annealing) typically occurring at 140−150 °C. Consequently, these fabrication processes will not just alter the morphology of the active layer but will also change the oxidation state of the metal electrode. Moreover, it should be possible to reverse certain degradation (oxidation) processes under the correct conditions with particular materials.

3. EXPERIMENTAL DETAILS

PSCs were prepared on cleaned ITO coated glass substrates with PEDOT:PSS as base material for hole transport and P3HT:PCBM as active layer. Prior to PEDOT:PSS deposition ITO substrates were subjected to UV-ozone treatment for 15 min. A thin layer of PEDOT:PSS was coated on ITO substrates by spin coating process at 4000 rpm for 90 s and dried at 140 °C for 30 min. The photoactive layer of the P3HT:PCBM blend (1:0.8) was spin coated from its chloroform solution (18 mg/mL) on the top of the PEDOT:PSS layer in a glovebox at 2000 rpm for 60 s and heated at 50 °C for 5 min. The samples were transferred to an evaporation chamber where cathode materials viz. Ca, Al, and Ag were deposited by thermal evaporation. This transportation resulted in an exposure of the samples to ambient air. Two sets of devices were prepared in ITO/PEDOT:PSS/P3HT:PCBM/Ca/Al and ITO/PEDOT:PSS/P3HT:PCBM/Ca/Ag structures. For all the devices Ca was maintained at 20 nm, whereas Al and Ag were deposited to 130 nm at ~2 × 10^{-6} mbar through shadow masks defining the cell area of 5 mm^2. After preparation all of the devices were subjected to thermal annealing at 140 °C for 5 min. The schematic structure of the solar cells is shown in the inset of Figure 3. The devices from each set were stored in dark in ambient

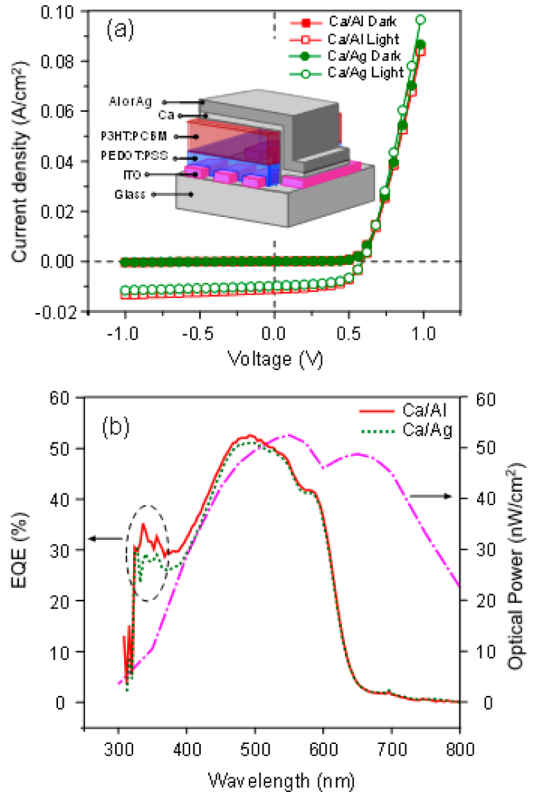

Figure 3. (a) Dark (solid symbols) and illuminated (open symbols) *J-V* characteristics of the fresh solar cells with Ca/Al and Ca/Ag cathodes. Inset: Schematic representation of the studied solar cells. (b) EQE graphs of the corresponding solar cells (solid and dashed lines) along with the optical power, incident on the cells (dash dotted line) for determination of EQE.

conditions (18 ± 3 °C, 55 ± 4% RH) without any protection or encapsulation and tested under 1 sun illumination of a 150W solar simulator with AM1.5G solar filter (Newport, USA). The experiments were conducted on a total of six solar cells for each electrode configuration. For subsequent analysis a subset of this data comprising the 3 highest performing fresh devices was used to ensure a conservative estimate of device recovery. Some of the devices from each set were placed under continuous illumination (40 mW/cm^2) of a W-halogen lamp in ambient air, and the *J-V* characteristics were collected every hour using a Keithley 2400 Source-Meter unit. XPS depth profiling analysis of the samples was performed using an ESCALAB250Xi with an incident Ar ion beam energy of 3 keV.

4. RESULTS AND DISCUSSION

In order to investigate the role of reversible and irreversible oxidation processes on PSC performance a series of devices with Ca/Al and Ca/Ag cathodes were fabricated and characterized: (i) as prepared ("fresh"), (ii) following exposure to ambient conditions for an extended period of time ("degraded"), and (iii) following heating a postdegraded device to 140 °C for 5 min in an inert atmosphere ("regenerated"). Figure 3 [parts (a) and (b), respectively] shows the dark and illuminated *J-V* characteristics and external quantum efficiency (EQE) for PSCs with Ca/Al and Ca/Ag cathodes. As expected, both the architectures exhibited similar device characteristics. Table 1 shows the photovoltaic parameters of fresh, degraded,

Table 1. Performance Characteristics for 1:0.8 P3HT:PCBM PSCs with Ca/Al and Ca/Ag Cathodes in the Fresh, Degraded, and Initially Regenerated States[a]

	J_{sc} (mA·cm^{-2})	V_{oc} (V)	*FF*	η (%)
Ca/Al fresh	9.96 (0.40)	0.59 (0.00)	0.58 (0.01)	3.44 (0.45)
Ca/Al degraded	0.08 (0.03)	0.57 (0.02)	0.29 (0.07)	0.05 (0.08)
Ca/Al regenerated	0.07 (0.02)	0.59 (0.00)	0.29 (0.05)	0.03 (0.04)
Ca/Ag fresh	9.33 (0.50)	0.58 (0.01)	0.57 (0.04)	3.08 (0.30)
Ca/Ag degraded	0.02 (0.01)	0.06 (0.01)	0.23 (0.01)	0.00 (0.00)
Ca/Ag regenerated	3.72 (0.41)	0.40 (0.10)	0.26 (0.03)	0.44 (0.12)

[a]Errors (shown in brackets) are calculated as the standard deviations for a set of 6 devices.

and regenerated solar cells with Ca/Al and Ca/Ag cathodes. PSCs containing a Ca/Ag electrode had a slightly lower EQE compared to those with Ca/Al electrodes, consistent with the difference in short circuit current density (J_{sc}) between the two devices (Table 1). Although both the device structures exhibited the same series resistance (R_s), devices with a Ca/Ag cathode had a slightly lower shunt resistance (R_{sh}) compared to those with a Ca/Al electrode, which corresponds to the lower J_{sc}, open circuit voltage (V_{oc}), and fill factor (*FF*) of the device with Ca/Ag electrode.[28]

Figure 4 shows the variation in normalized photovoltaic parameters of typical PSCs having Ca/Al and Ca/Ag cathodes and stored in the dark between measurements. Both structures exhibit an exponential decay in efficiency as a function of time. Devices with Ca/Al and Ca/Ag electrodes degrade to half of their initial efficiency in ~55 h and in ~42 h, respectively. For both architectures, there is little or no change in V_{oc} and *FF* up to 50 h of degradation, and up to this time the decrease in efficiency arises purely because of a reduction in J_{sc}. The key difference in performance between the two architectures is the abrupt decrease in V_{oc}, which occurs after ~100 h of degradation for only the Ca/Ag cathode. The fact that the transition is only observed for the Ca/Ag cathode and not the Ca/Al cathode suggests that the change is independent of the Ca layer and arises from the presence of the Ag electrode. Moreover, the observation of an abrupt transition in V_{oc} that is independent of the monotonic decrease in J_{sc} indicates that this process is most likely associated with the creation of an

dx.doi.org/10.1021/am500637n | ACS Appl. Mater. Interfaces 2014, 6, 5281−5289

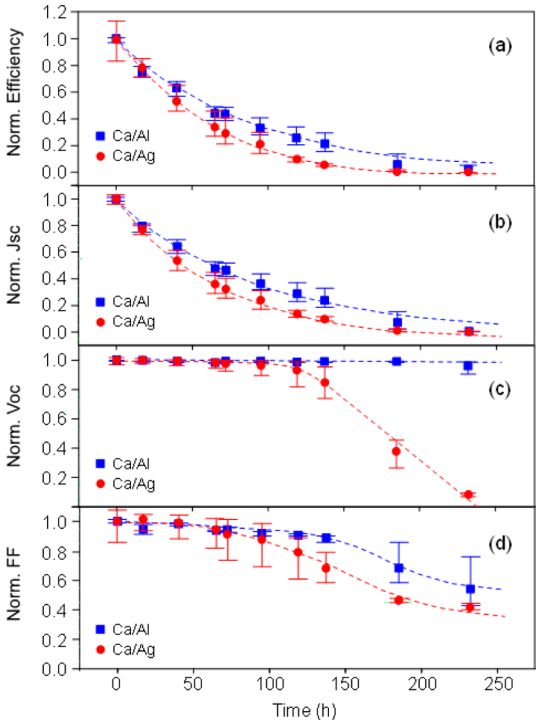

Figure 4. Degradation in (a) normalized efficiency, (b) normalized J_{sc}, (c) normalized V_{oc}, and (d) normalized *FF*, of the PSCs with Ca/Al and Ca/Ag electrodes. The data and error bars are calculated from the average and standard deviation values for the 3 highest efficiency fresh devices presented in Table 1.

interfacial surface state. Ag forms a thin passivating conductive native oxide layer that is only 1−3 nm thick,[29] and upon oxidation its work function increases from 4.3 to 5.0 eV.[30] Thus, given that the work function of the ITO/PEDOT:PSS anode is around 5 eV, silver oxide's increased work function should lead to the formation of an interfacial surface state that will tend to reduce the V_{oc} of the device. Indeed, this hypothesis is strongly supported by work by Kim et al. who report V_{oc} reversal upon silver electrode oxidation in P3HT:PCBM devices.[30] Therefore, the drop in V_{oc} observed after ∼100 h of degradation is entirely consistent with the formation of a partial silver oxide interfacial layer.

Devices with Ca/Al and Ca/Ag cathodes were also tested under continuous illumination in ambient conditions, and the degradation graphs are shown in Figure 5. Both architectures exhibit first a rapid and then a slow linear degradation in efficiency. Indeed, an initial rapid degradation in all of the photovoltaic parameters was observed. The solar cell with Ca/Ag electrodes degraded relatively faster compared to those with Ca/Al electrodes, which is the same behavior as observed previously for those stored in dark (Figure 4). Significantly, V_{oc} remained constant even after ∼230 h of degradation for both device architectures. The absence of an abrupt drop in V_{oc} after ∼100 h indicates that under constant illumination the interfacial silver oxide layer does not occur within the time scale of the experiment. We postulate that the increased device temperature (∼58 °C) that arises due to the continuous illumination results in a reduced driving force for silver oxidation in agreement with the Ellingham diagram for this process (Figure 1). As such, these observations indicate that heating to higher temperatures will retard silver cathode

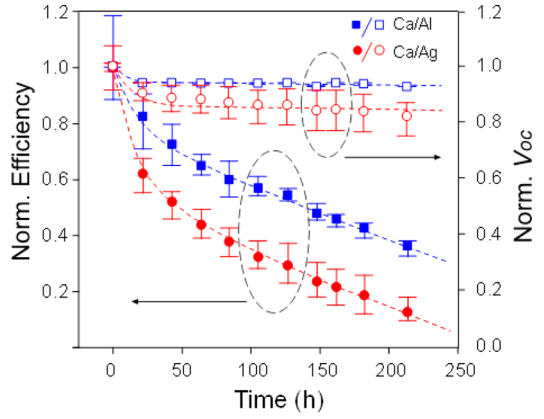

Figure 5. Degradation in normalized efficiency and normalized V_{oc} of the solar cells with Ca/Al and Ca/Ag electrodes and tested under continuous illumination of a W-halogen lamp at an irradiance of 40 mW/cm^2. The data and error bars are calculated from the average and standard deviation values for the 3 highest efficiency fresh devices presented in Table 1.

degradation or potentially even reverse the oxidation process completely.

In order to test the reversibility of these oxidation processes, fully degraded devices with Ca/Al and Ca/Ag cathodes were subsequently heated at 140 °C for 5 min in an inert atmosphere. Figure 6 (a) shows the degradation profiles of efficiency (η) and V_{oc} following repeated heating cycles in an inert atmosphere for fully degraded solar cells with a Ca/Ag cathode, which were stored in the dark between measurements. Figure 6 (b) shows the corresponding profiles for J_{sc} and *FF*. It is clear from Figure 6 that each heating cycle leads to a

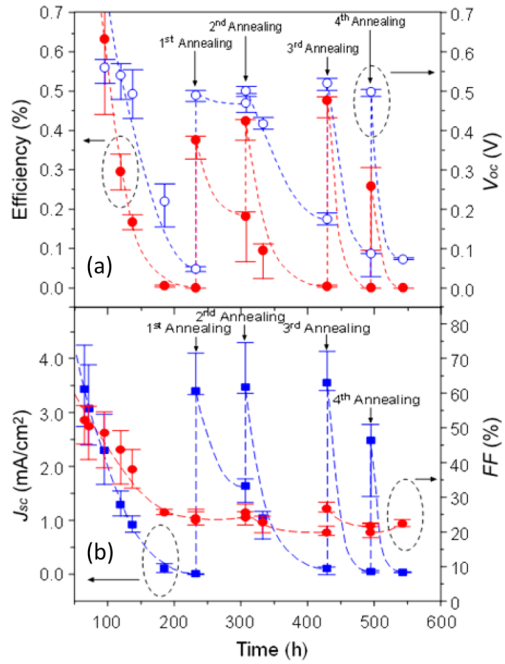

Figure 6. Effect of repeated heating cycles in an inert atmosphere on fully degraded devices with Ca/Ag cathodes: (a) variation of η and V_{oc} and (b) variation of J_{sc} and *FF*. Dashed lines are drawn to guide the eye to the trends in data. The data and error bars are calculated from the average and standard deviation values for the 3 highest efficiency fresh devices presented in Table 1.

dx.doi.org/10.1021/am500637n | ACS Appl. Mater. Interfaces 2014, 6, 5281−5289

significant increase in V_{oc} and J_{sc}, resulting in a reproducible recovery in η of 12−15% every regeneration cycle.

By comparison, Figure 7 shows the effect of heating cycles on J_{sc} and V_{oc} for degraded solar cells with Ca/Al cathodes.

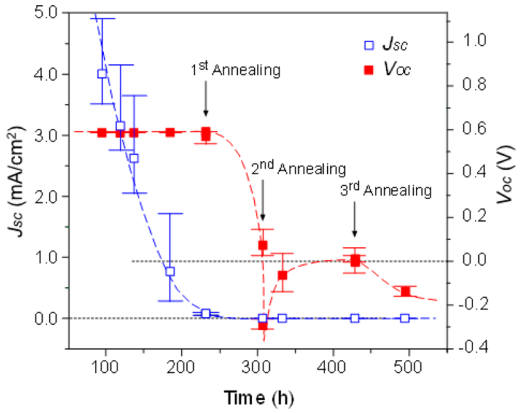

Figure 7. Effect of thermal annealing at different time intervals and further degradation in J_{sc} and V_{oc} of the solar cells with Ca/Al cathodes. Dashed lines are drawn to guide the eye to the trends in data. The data and error bars are calculated from the average and standard deviation values for the 3 highest efficiency fresh devices presented in Table 1.

Interestingly, despite the fact that the solar cells with Ca/Al cathodes were functionally fully degraded after 230 h of exposure, V_{oc} retained the same value as the as-prepared devices. However, after the first heating cycle, V_{oc} degraded very quickly and J_{sc} was further reduced. After the second heating cycle the dark illuminated *J-V* characteristics started passing through the second quadrant which resulted into negative V_{oc} and J_{sc} and can be attributed to further degradation.[31]

Figure 8 shows the EQE spectra of degraded devices with Ca/Ag and Ca/Al electrodes before and after the first heating

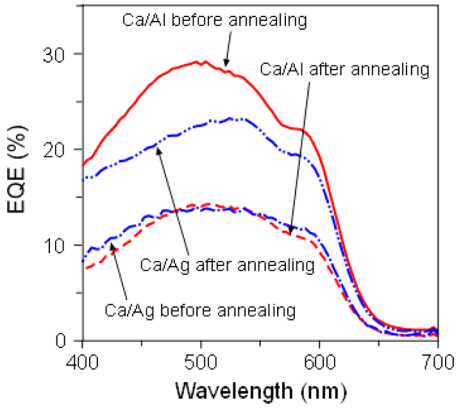

Figure 8. Effect of thermal annealing on the EQE of the solar cells with Ca/Al and Ca/Ag electrodes.

cycle. As expected, devices with Ca/Ag electrodes exhibited an overall increase in EQE after the first heating cycle, whereas those with Ca/Al electrodes exhibited reduction in EQE, consistent with the observed variation in J_{sc}. Moreover, there is no significant change to the shape of the EQE plots, both before and after the heating cycle and for the different electrode materials. This observation suggests that improved response upon heating a degraded device does not arise from a change in the crystallinity of the P3HT material or from a change in the relative contribution from the two components in the active layer, both of which would change the shape of the EQE plots.[32]

In order to determine the threshold temperature for the recovery process, degraded Ca/Ag devices were subject to a series of heating cycles at different temperatures. Figure 9

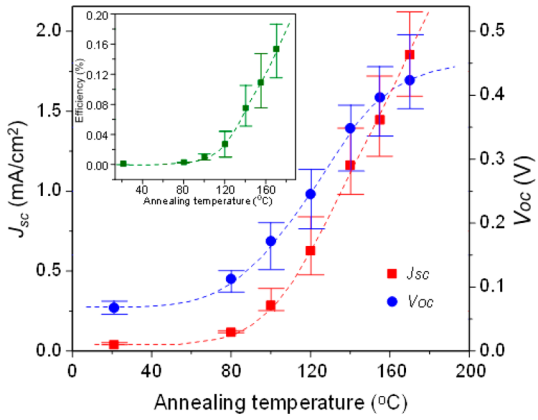

Figure 9. Effect of annealing temperature on J_{sc} and V_{oc} of the regenerated solar cells with Ca/Ag electrodes. Inset: The corresponding effect of annealing temperature on efficiency of the same devices. Dashed lines are drawn to guide the eye to the trends in data. The data and error bars are calculated from the average and standard deviation values for 3 devices.

shows that J_{sc} and V_{oc} increase gradually with heating temperature, and since there is no significant effect on *FF* (not shown), η also increases systematically. Importantly, V_{oc} was observed to approach an asymptote at higher annealing temperatures, and this limiting V_{oc} value was less than that of the as-prepared devices.

To further probe the regeneration of solar cells with Ca/Ag electrodes we analyzed their dark and illuminated *J-V* characteristics before and after each heating cycle (Figure 10). It can be seen that for the devices measured after each heating cycle, the illuminated *J-V* characteristics intersect their corresponding dark *J-V* characteristics at a common voltage (0.56 V), whereas the characteristics measured before each heating cycle did not exhibit a common intersection point. The intersection point of the dark and illuminated *J-V* characteristics is related to the built-in voltage (V_{bi}) of the devices, and thus the common intersection point indicates that the device recovers to the same V_{bi} after every heating cycle.[33,34] Since V_{bi} is determined mainly by the interfacial properties at the electrodes[35,36] and that the recovery is only observed for the Ca/Ag electrode devices, these results suggest that the device recovery is driven primarily by changes at the Ca/Ag electrode interface.

In order to probe the changes occurring at the Ca/Ag electrode interfaces, a detailed XPS depth profiling analysis of fresh, degraded, and regenerated solar cells was conducted. The composition as a function of depth was tracked by measuring the change in the area of the elemental XPS peak relevant to the component of interest. Thus, the silver and calcium layers are directly identified by measuring the silver and calcium 2p peaks, the active layer is identified from the carbon 1s peak, and the anode is tracked by looking at the indium $3d_{5/2}$ peak. In addition, by monitoring the sulfur 2p signal and the carbon:sulfur (C:S) ratio, it is possible to monitor both the

dx.doi.org/10.1021/am500637n | ACS Appl. Mater. Interfaces 2014, 6, 5281−5289

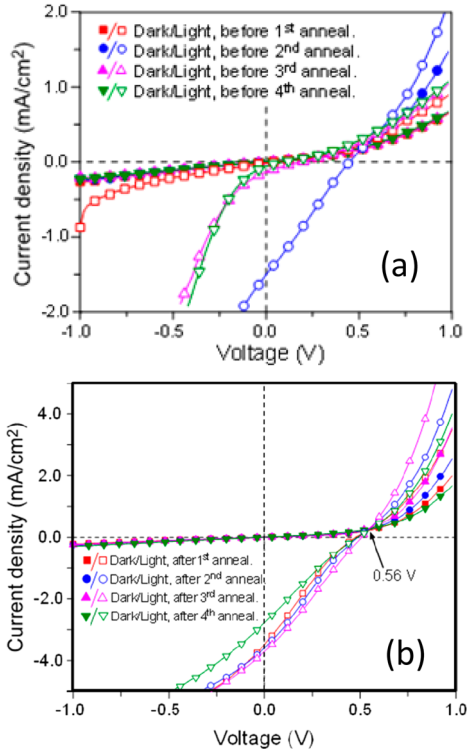

Figure 10. (a) Dark (solid) and illuminated (open) *J-V* characteristics of a typical solar cell with Ca/Ag electrodes before each heating cycle. (b) Dark (solid) and illuminated (open) *J-V* characteristics of solar cell with Ca/Ag electrodes after each heating cycle (140 °C for 5 min). The samples were stored in the dark between measurements.

relative P3HT:PCBM concentration and to differentiate between the active and PEDOT:PSS layers.[37,38] Figure 11 shows the XPS elemental depth profile analysis of (a) fresh, (b) degraded, and (c) regenerated solar cells with Ca/Ag cathodes. For all three devices, the carbon concentration is higher at the cathode suggesting that PCBM has segregated to the top electrode, consistent with previous studies.[39] This observation provides further confirmation that changes in the active layer are not the primary cause for the observed changes in device performance upon degradation and regeneration.

At the anode interface, the In $3d_{5/2}$, O 1s, and Si 2p peaks all broaden after the regeneration process indicating that the anode interface becomes less distinct. However, we observe that an O 1s peak is also located at the cathode interface coincident with the position of the Ca 1s peak. Moreover, it is apparent that this O 1s peak increases upon degradation and again (to a lesser extent) upon regeneration consistent with oxidative degradation of the cathode.

Previous work has shown that Ca deposition onto P3HT layers results in the formation of CaS islands at the Ca/P3HT interface as evidenced by the presence of a low energy (~161.7 eV) sulfide component to the S 2p spectrum.[40] Figure 12 shows the S 2p spectrum at the peak of the calcium interface signal in the depth profile (Figure 11) for the fresh, degraded, and regenerated devices. While the count rates for all three samples are low (since the Ca interfacial region is only 20 nm thick) the signal:noise ratio is sufficient to draw reasonable conclusions from the peak fitting. All three plots clearly show the presence of two sulfur species, with the lower and higher energy fitted peaks corresponding to the sulfide and P3HT components, respectively, indicating that CaS is indeed present at the

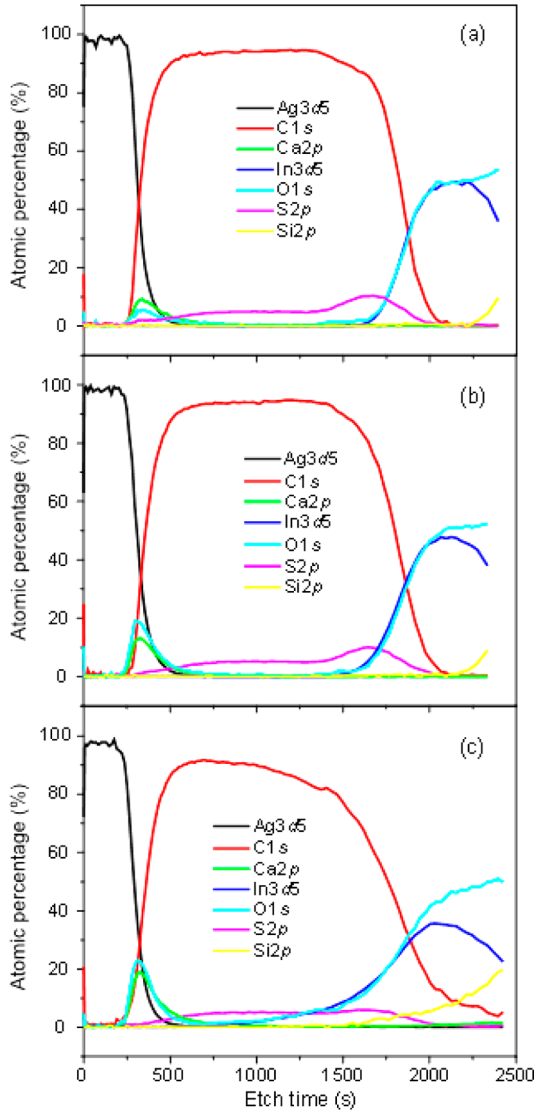

Figure 11. Elemental XPS depth profiles of (a) fresh, (b) degraded, and (c) regenerated PSCs with a Ca/Ag cathode.

interface. Upon degradation and subsequent regeneration we observe a decrease in the sulfur signal (consistent with the depth profiles) and, more importantly, a change in ratio of the two peaks with the sulfide contribution systematically decreasing. This observation is consistent with the systematic loss of CaS, which can be explained by the initial formation of mixed hydroxythiol species and subsequent loss of H_2S to form $Ca(OH)_2$:[41]

$$CaS + H_2O \rightarrow Ca(SH)(OH) + H_2O \rightarrow Ca(OH)_2 + H_2S \quad (9)$$

To further probe the speciation of oxidation products at the cathode interface, the O:Ca ratios are plotted in Figure 13. The data for the fresh device shows an effectively constant O:Ca ratio across the interface region with a ratio value of ~0.5. This value is consistent with the presence of a mixed layer containing Ca, CaO, and CaS, where the oxidized species makes up about 50% of the total Ca content. Upon degradation, the O:Ca ratio systematically increases to a value of 1.3−1.6 across the interface region. The observation of an O:Ca ratio greater than 1 necessarily implies the further oxidation of Ca to form a

dx.doi.org/10.1021/am500637n | ACS Appl. Mater. Interfaces 2014, 6, 5281−5289

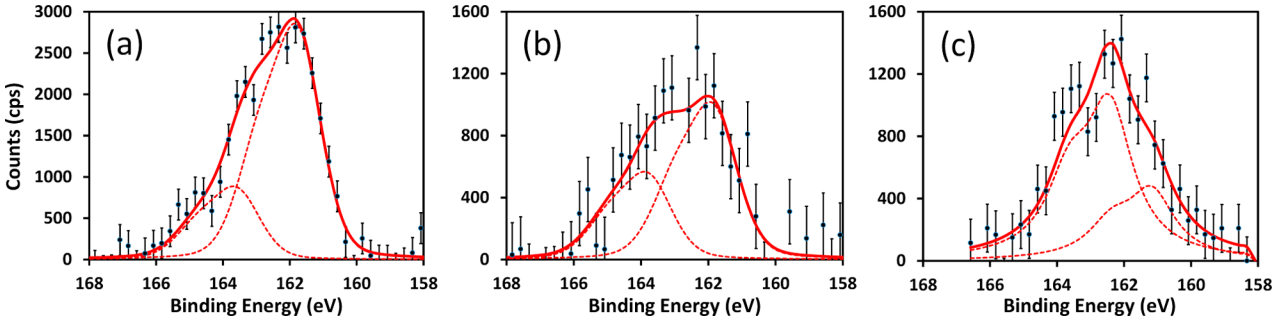

Figure 12. Elemental S 2p XPS spectra at the peak of the Ca interface signal in the depth profiles of (a) fresh, (b) degraded, and (c) regenerated PSCs with a Ca/Ag cathode. The S 2p peaks are fitted with a spin orbit splitting of 1.2 eV, and the error bars are calculated from the standard deviation of the differences between the experimental and fitted data across all of the energies of the S 2p spectra.

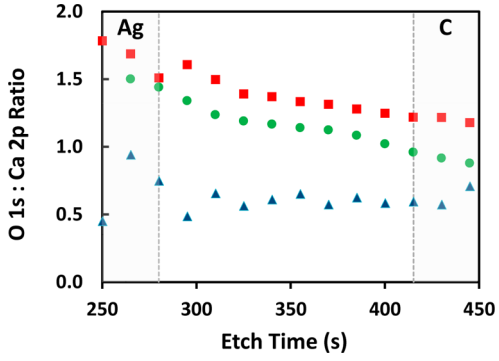

Figure 13. O 1s:Ca 2p XPS ratios in the cathode/active layer interface region for fresh (blue triangles), degraded (red squares), and regenerated (green circles) PSCs with a Ca/Ag cathode. The region marked Ag denotes the bulk silver region with the dashed line denoting the Ag/Ca interface defined by the 80% Ag concentration level. The region marked C denotes the bulk carbon region with the dashed line denoting the Ca/active layer interface defined by the 80% C concentration level.

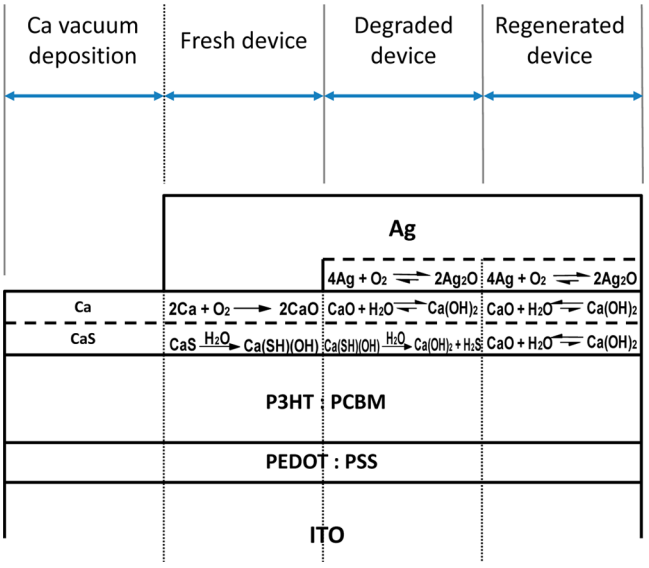

Figure 14. Schematic diagram illustrating the thermodynamic reaction processes that occur upon during the vacuum deposition of a Ca/Ag to form a "fresh" polymer solar cell and during subsequent degradation under ambient conditions and regeneration in an inert atmosphere glovebox at 140 °C.

mixed oxide layer, which must now contain $Ca(OH)_2$. Upon regeneration, the O:Ca ratio is systemically reduced across the interface region, falling to a value of 1.0−1.5, which is consistent with the thermal dehydration of $Ca(OH)_2$ to CaO.

5. MODEL FOR CATHODE DEGRADATION IN POLYMER SOLAR CELLS

In light of these measurements, it is now possible to develop an overall model for the oxidative processes at Ca/Ag and Ca/Al cathodes. Initially, vacuum deposition of Ca onto the P3HT:PCBM active layer results in the formation of a Ca layer overlying CaS islands at the Ca/active layer interface (see Figure 14). Vacuum deposition of a Ag layer on top of the Ca acts as a barrier to oxygen and water, while the Ca layer prevents the formation of AgS. Even for the "fresh" sample, oxygen and water diffusion occurs (either upon exposure to ambient air or from entrapped water), and partial oxidation of the remaining calcium electrode occurs.

Upon degradation in a moist air atmosphere (moderate RH), oxygen and water diffusion continues, and the calcium layer is fully converted to oxide and then to a mixed oxide/hydroxide layer. As the Ca becomes fully oxidized (with more complete conversion to $Ca(OH)_2$), then oxidation of the Ag (or Al) electrode occurs. The native Ag oxide is thin (1−2 nm) due to self-passivation of the oxide growth, and a complete layer is not obtained since electronic inversion of the device function is not observed. The Al forms a thicker oxide which also acts to passivate the cathode surface.[29] In addition, the gradual conversion of CaS into CaO and subsequently to $Ca(OH)_2$ via the formation of mixed hydroxythiol species (Ca(SH)-(OH)) takes place. Finally, upon regeneration at 140 °C in the glovebox, there are two thermodynamic processes that occur. First, the silver oxide starts to convert back to Ag, as evidenced by the recovery of V_{oc}. Second, under a nitrogen atmosphere, the $CaO/Ca(OH)_2$ equilibrium temperature is lowered to ∼150 °C, and thus the equilibrium is shifted to favor the dehydration of $Ca(OH)_2$. In the case of the Ca/Al cathode, however, the aluminum oxidation is irreversible, and hence no recovery of device performance is possible.

6. CONCLUSION

A comparative study of the degradation of PSCs with two different cathodes (Ca/Al and Ca/Ag) is reported. A significant source of degradation in these devices lies in the oxidation of the metal cathode. The thermodynamics of these oxidation processes is complex and governed by a number of irreversible and reversible reactions. In line with predictions based on the known chemical thermodynamics of the cathode materials, we

show that degraded PSCs with the two different cathodes behave very differently when subjected to thermal annealing under inert atmosphere. In particular, PSCs based on a Ca/Ag cathode exhibited considerable device recovery, whereas those with a Ca/Al cathode deteriorated further. The regeneration of the Ca/Ag PSCs arises primarily due to the reduction of Ag_2O back to Ag. However, in the case of the Ca/Al cathode, degradation and regeneration both result in irreversible oxidation of the Al electrode to produce a layer of insulating Al_2O_3, which inhibits the extraction of charge carriers and the performance deteriorates. Here we demonstrate that a ∼15% recovery in device efficiency is possible through a simple thermal treatment of a Ca/Ag cathode. Since there are other degradation processes occurring (such as the anode degradation identified in this paper), we can conclude that a minimum of 15% of the total degradation originates from oxidation of the cathode.

AUTHOR INFORMATION

Corresponding Authors

*E-mail: pankaj@mail.nplindia.ernet.in.

*E-mail: Paul.Dastoor@newcastle.edu.au.

Notes

The authors declare no competing financial interest.

ACKNOWLEDGMENTS

The University of Newcastle is gratefully acknowledged for a Ph.D. scholarship (N.N.). One of the authors (P.K.) is grateful to the Indian National Science Academy (INSA), New Delhi, for the award of an Early Career Indo-Australia research fellowship to pursue this work in Australia. This project is supported by the Australian Government, through the Australian Renewable Energy Agency (K.F.). This work was performed in part at the Materials node of the Australian National Fabrication Facility, a company established under the National Collaborative Research Infrastructure Strategy to provide nano- and microfabrication facilities for Australia's researchers.

REFERENCES

(1) Kumar, P.; Chand, S. Recent Progress and Future Aspects of Organic Solar Cells. *Prog. Photovolt.: Res. Appl.* **2012**, *20*, 377−415.

(2) Liang, Y.; Xu, Z.; Xia, J.; Tsai, S. T.; Wu, Y.; Li, G.; Ray, C.; Yu, L. For the Bright Future-Bulk Heterojunction Polymer Solar Cells with Power Conversion Efficiency of 7.4%. *Adv. Mater.* **2010**, *22*, E135−E138.

(3) www.solarmer.com, http://pv-tech.org/news/_c/opv_dssc (accessed March 15, 2014).

(4) You, J.; Dou, L.; Yoshimura, K.; Kato, T.; Ohya, K.; Moriarty, T.; Emery, K.; Chen, C. C.; Gao, J.; Li, G.; Yang, Y. A Polymer Tandem Solar Cell with 10.6% Power Conversion Efficiency. *Nat. Commun.* **2013**, *4*, 1446 1−10.

(5) You, J.; Chen, C. C.; Hong, Z.; Yoshimura, K.; Ohya, K.; Xu, R.; Ye, S.; Gao, J.; Li, G.; Yang, Y. 10.2% Power Conversion Efficiency Polymer Tandem Solar Cells Consisting of Two Identical Sub-Cells. *Adv. Mater.* **2013**, *25*, 3973−3978.

(6) He, Z.; Zhong, C.; Su, S.; Xu, M.; Wu, H.; Cao, Y. Enhanced Power-Conversion Efficiency in Polymer Solar Cells Using an Inverted Device Structure. *Nat. Photonics* **2012**, *6*, 591−595.

(7) Amb, C. M.; Chen, S.; Graham, K. R.; Subbiah, J.; Small, C. E.; So, F.; Reynolds, J. R. Dithienogermole As a Fused Electron Donor in Bulk Heterojunction Solar Cells. *J. Am. Chem. Soc.* **2011**, *133*, 10062−10065.

(8) Dennler, G.; Scharber, M. C.; Brabec, C. J. Polymer-Fullerene Bulk-Heterojunction Solar Cells. *Adv. Mater.* **2009**, *21*, 1323−1338.

(9) Dennler, G.; Brabec, C. J. *Organic Photovoltaics: Materials, Device Physics, and Manufacturing Technologies*; Wiley-VCH: Weinheim, 2008.

(10) Jorgensen, M.; Norrman, K.; Gevorgyan, S. A.; Tromholt, T.; Andreasen, B.; Krebs, F. C. Stability of Polymer Solar Cells. *Adv. Mater.* **2012**, *24*, 580−612.

(11) Chambon, S.; Rivaton, A.; Gardette, J. L.; Firon, M. Photo and Thermal Degradation of MDMO-PPV:PCBM Blends. *Sol. Energy Mater. Sol. Cells* **2007**, *91*, 394−398.

(12) Padinger, F.; Fromherz, T.; Denk, P.; Brabec, C. J.; Zettner, J.; Hierl, T.; Sariciftci, N. S. Degradation of Bulk Heterojunction Solar Cells Operated in an Inert Gas Atmosphere: A Systematic Study. *Synth. Met.* **2001**, *121*, 1605−1606.

(13) Norrman, K.; Madsen, M. V.; Gevorgyan, S. A.; Krebs, F. C. Degradation Patterns in Water and Oxygen of an Inverted Polymer Solar Cell. *J. Am. Chem. Soc.* **2010**, *132*, 16883−16892.

(14) Yang, H. B.; Song, Q. L.; Gong, C.; Li, C. M. The Degradation of Indium Tin Oxide/Pentacene/Fullerene/Tris-8-hydroxy-quinolina-to Aluminum/Aluminum Heterojunction Organic Solar Cells: By Oxygen or Moisture? *Sol. Energy Mater. Sol. Cells* **2010**, *94*, 846−849.

(15) Yang, X.; van Duren, J. K. J.; Janssen, R. A. J.; Michels, M. A. J.; Loos, J. Morphology and Thermal Stability of the Active Layer in Poly(*p*-phenylenevinylene)/Methanofullerene Plastic Photovoltaic Devices. *Macromolecules* **2004**, *37*, 2151−2158.

(16) Gevorgyan, S. A.; Krebs, F. C. Bulk Heterojunctions Based on Native Polythiophene. *Chem. Mater.* **2008**, *20*, 4386−4390.

(17) Gallardo, D. E.; Bertoni, C.; Dunn, S.; Gaponik, N.; Eychmüller, A. Cathodic and Anodic Material Diffusion in Polymer/Semiconductor-Nanocrystal Composite Devices. *Adv. Mater.* **2007**, *19*, 3364−3367.

(18) Hintz, H.; Egelhaaf, H. J.; Luer, L.; Hauch, J.; Peisert, H.; Chasse, T. Photodegradation of P3HT−A Systematic Study of Environmental Factors. *Chem. Mater.* **2011**, *23*, 145−154.

(19) Krebs, F. C.; Gevorgyan, S. A.; Alstrup, J. A Roll-to-Roll Process to Flexible Polymer Solar Cells: Model Studies, Manufacture and Operational Stability Studies. *J. Mater. Chem.* **2009**, *19*, 5442−5451.

(20) Norrman, K.; Larsen, N. B.; Krebs, F. C. Lifetimes of Organic Photovoltaics: Combining Chemical and Physical Characterization Techniques To Study Degradation Mechanisms. *Sol. Energy Mater. Sol. Cells* **2006**, *90*, 2793−2814.

(21) Krebs, F. C.; Norrman, K. Analysis of the Failure Mechanism for a Stable Organic Photovoltaic During 10000 h of Testing. *Prog. Photovolt.: Res. Appl.* **2007**, *15*, 697−712.

(22) Norrman, K.; Gevorgyan, S. A.; Krebs, F. C. Water-Induced Degradation of Polymer Solar Cells Studied by $H_2{}^{18}O$ Labeling. *ACS Appl. Mater. Interfaces* **2009**, *1*, 102−112.

(23) Feron, K.; Nagle, T. J.; Rozanski, L. J.; Gong, B. B.; Fell, C. J. Spatially Resolved Photocurrent Measurements of Organic Solar Cells: Tracking Water Ingress at Edges and Pinholes. *Sol. Energy Mater. Sol. Cells* **2013**, *109*, 169−177.

(24) Devi, T. G.; Kannan, M. P. X-ray Diffraction (XRD) Studies on the Chemical States of Some Metal Species in Cellulosic Chars and the Ellingham Diagrams. *Energy Fuels* **2007**, *21*, 596−601.

(25) Getman, R. B.; Xu, Y.; Schneider, W. F. Thermodynamics of Environment-Dependent Oxygen Chemisorption on Pt(111). *J. Phys. Chem. C* **2008**, *112*, 9559−9572.

(26) Reese, M. O.; Dameron, A. A.; Kempe, M. D. Quantitative Calcium Resistivity Based Method for Accurate and Scalable Water Vapor Transmission Rate Measurement. *Rev. Sci. Instrum.* **2011**, *82*, 85101 1−11.

(27) Schaube, F.; Koch, L.; Wörner, A.; Steinhagen, H. M. A Thermodynamic and Kinetic Study of the De- and Rehydration of $Ca(OH)_2$ at High H_2O Partial Pressures for Thermo-Chemical Heat Storage. *Thermochim. Acta* **2012**, *538*, 9−20.

(28) Gaur, A.; Kumar, P. An Improved Circuit Model for Polymer Solar Cells. *Prog. Photovolt.: Res. Appl.* **2013**, DOI: 10.1002/pip.2345.

(29) Over, H.; Seitsonen, A. P. Oxidation of Metal Surfaces. *Science* **2002**, *297*, 2003−2005.

(30) Kim, J. B.; Kim, C. S.; Kim, Y. S.; Loo, Y. L. Oxidation of Silver Electrodes Induces Transition from Conventional to Inverted

Photovoltaic Characteristics in Polymer Solar Cells. *Appl. Phys. Lett.* **2009**, *95*, 1833011−4.
(31) Kumar, P.; Sharma, A.; Singh, D. P. Effect of Voltage Sweep Direction on the Performance Evaluation of P3HT: PCBM Solar Cells. *Prog. Photovolt.: Res. Appl.* **2013**, *21*, 950−959.
(32) Nicolaidis, N.; Routley, B.; Holdsworth, J.; Belcher, W.; Zhou, X.; Dastoor, P. Fullerene Contribution to Photocurrent Generation in Organic Photovoltaic Cells. *J. Phys. Chem. C* **2011**, *115*, 7801−7805.
(33) Kumar, P.; Jain, S. C.; Kumar, H.; Chand, S.; Kumar, V. Effect of Illumination Intensity and Temperature on Open Circuit Voltage in Organic Solar Cells. *Appl. Phys. Lett.* **2009**, *94*, 183505 1−4.
(34) Kumar, P.; Gaur, A. Model for the *J-V* Characteristics of Degraded Polymer Solar Cells. *J. Appl. Phys.* **2013**, *113*, 94505 1−9.
(35) Luo, J.; Wu, H.; He, C.; Li, A.; Yang, W.; Cao, Y. Enhanced Open-Circuit Voltage in Polymer Solar Cells. *Appl. Phys. Lett.* **2009**, *95*, 43301 1−4.
(36) Zhang, T.; Huang, J.; Hea, F.; Chen, L.; Niu, G.; Pan, J.; Song, Q. The Effect of Built-in Field on the Interface Exciton Recombination and Dissociation in N-N Type Organic Solar Cells. *Sol. Energy Mater. Sol. Cells* **2013**, *112*, 73−77.
(37) Xu, Z.; Chen, L. M.; Yang, G.; Huang, C. H.; Hou, J.; Wu, Y.; Li, G.; Hsu, C. S.; Yang, Y. Vertical Phase Separation in Poly(3-hexylthiophene): Fullerene Derivative Blends and Its Advantage for Inverted Structure Solar Cells. *Adv. Funct. Mater.* **2009**, *19*, 1227−1234.
(38) Ma, S. Y.; Shen, Y. M.; Yang, P. C.; Chen, C. S.; Lin, C. F. Morphological Modification Induced by External Electric Field During Solution Process of Organic Solar Cells. *Org. Electron.* **2012**, *13*, 297−301.
(39) Feron, K.; Fell, C. J.; Rozanski, L. J.; Gong, B. B.; Nicolaidis, N.; Belcher, W. J.; Zhou, X.; Sesa, E.; King, B. V.; Dastoor, P. C. Towards the Development of a Virtual Organic Solar Cell: An Experimental and Dynamic Monte Carlo Study of the Role of Charge Blocking Layers and Active Layer Thickness. *Appl. Phys. Lett.* **2012**, *101*, 193306 1−6.
(40) Bebensee, F.; Schmid, M.; Steinrück, H. P.; Campbell, C. T.; Gottfried, J. M. Toward Well-Defined Metal−Polymer Interfaces: Temperature-Controlled Suppression of Subsurface Diffusion and Reaction at the Calcium/Poly(3-Hexylthiophene) Interface. *J. Am. Chem. Soc.* **2010**, *132*, 12163−12165.
(41) Ropp, R. C. *Encyclopedia of the Alkaline Earth Compounds*; Elsevier: Oxford, UK, 2013.